EMORY LIBRARIES & INFORMATION TECHNOLOGY | OpenEmory

# Combination of an Integrin-Targeting NIR Tracer and an Ultrasensitive Spectroscopic Device for Intraoperative Detection of Head and Neck Tumor Margins and Metastatic Lymph Nodes.

Younghyoun Yoon, *Emory University*
Aaron M. Mohs, *Georgia Institute of Technology*
Michael C. Mancini, *Georgia Institute of Technology*
Shuming Nie, *Emory University*
Hyunsuk Shim, *Emory University*

**Journal Title:** Tomography : a journal for imaging research
**Volume:** Volume 2, Number 3
**Publisher:** Grapho Publications, LLC. | 2016-09, Pages 215-222
**Type of Work:** Article | Final Publisher PDF
**Publisher DOI:** 10.18383/j.tom.2016.00253
**Permanent URL:** https://pid.emory.edu/ark:/25593/rrrv0

Final published version: http://dx.doi.org/10.18383/j.tom.2016.00253

## Copyright information:

This is an Open Access work distributed under the terms of the Creative Commons Attribution-NonCommercial-NoDerivatives 4.0 International License (http://creativecommons.org/licenses/by-nc-nd/4.0/).

*Accessed October 15, 2019 6:44 PM EDT*

# Combination of an Integrin-Targeting NIR Tracer and an Ultrasensitive Spectroscopic Device for Intraoperative Detection of Head and Neck Tumor Margins and Metastatic Lymph Nodes

**Younghyoun Yoon[1], Aaron M. Mohs[2,3], Michael C. Mancini[2], Shuming Nie[2], and Hyunsuk Shim[1,2,4]**

[1]Department of Radiology and Imaging Science, Emory University School of Medicine, Atlanta, Georgia; [2]Department of Biomedical Engineering, Emory University and Georgia Institute of Technology, Atlanta, Georgia; [3]Department of Pharmaceutical Sciences, University of Nebraska Medical Center, Omaha, Nebraska; and [4]Winship Cancer Institute, Emory University, Atlanta, Georgia

**Corresponding Author:** Hyunsuk Shim, PhD
Department of Radiology and Imaging Sciences,
1701 Uppergate Drive, C5018, Atlanta, GA 30322
E-mail: hshim@emory.edu

**Key Words:** intraoperative guidance, near-infrared, RGD, infiltrative, metastatic, head and neck cancer, tumor margins, lymph nodes

**Abbreviations:** Squamous cell carcinoma (SCC), SCC head and neck (SCCHN), hematoxylin and eosin (H&E), Food and Drug Administration (FDA), positron emission tomography (PET), phosphate buffered saline (PBS), near-infrared (NIR), signal-to-noise ratio (SNR), epidermal growth factor receptor (EGFR)

ABSTRACT

Despite major advances in targeted drug therapy and radiation therapy, surgery remains the most effective treatment for most solid tumors. The single most important predictor of patient survival is a complete surgical resection of the primary tumor, draining lymph nodes, and metastatic lesions. Presently, however, 20%–30% of patients with head and neck cancer who undergo surgery still leave the operating room without complete resection because of missed lesions. Thus, major opportunities exist to develop advanced imaging tracers and intraoperative instrumentation that would allow surgeons to visualize microscopic tumors during surgery. The cell adhesion molecule integrin $\alpha v\beta 3$ is specifically expressed by tumor neovasculature and invading tumor cells, but not by quiescent vessels or normal cells. Here we report the combined use of an integrin-targeting near-infrared tracer (RGD-IRDye800CW) and a handheld spectroscopic device, an integrated point spectroscopy with wide-field imaging system, for highly sensitive detection of integrin overexpression on infiltrating cancer cells. By using an orthotopic head and neck cancer animal model, we show that this tracer–device combination allows intraoperative detection of not only invasive tumor margins but also metastatic lymph nodes. Correlated histological analysis further reveals that microscopic clusters of 50–100 tumor cells can be detected intraoperatively with high sensitivity and specificity, raising new possibilities in guiding surgical resection of microscopic tumors and metastatic lymph nodes.

## INTRODUCTION

Squamous cell carcinoma (SCC) is a malignant tumor of epithelial origin. More than 90% of all head and neck cancers are SCC (1). About 60% of patients with SCC head and neck (SCCHN) cancer have lymph node metastases, whereas ~20% to 25% of patients with SCCHN have developed distant metastases primarily in the lungs (2). Oral SCC comprises 2%–3% of all new malignancies diagnosed in the USA, and it is the 10th most common malignancy. However, during the last a few decades, the average 5-year survival rate of 50% has not changed despite advances in surgical and medical therapies (3).

Ravasz et al. examined the relation of local recurrence with the presence or absence of tumors at the surgical margin, which was combined with other indications of postoperative radiotherapy (4). Local recurrence was observed in 20% of patients and was correlated with tumor thickness over 5 mm, spidery growth, and tumor-positive margins. Standardized reporting of head and neck cancer resections, according to guidelines issued by the UK Royal College of Pathologists, was introduced as a routine procedure in 1998 (5). They reported the frequency, type, and morphological features of involved margins and assessed the influence of tumor site and pathological tumor and node stages from 301 radical resection specimens for oral/oropharyngeal SCC (cases from 1998 to 2005). Seventy resections (23%) had involved margins, and the frequency was related to the primary tumor site and pathological tumor and node stages. It is reasonable to assume that large tumors are more difficult to resect, given the anatomical restraints at many sites within the

© 2016 The Authors. Published by Grapho Publications, LLC This is an open access article under the CC BY-NC-ND license (http://creativecommons.org/licenses/by-nc-nd/4.0/).
ISSN 2379-1381 http://dx.doi.org/10.18383/j.tom.2016.00253

oral cavity and oropharynx. An involved, deep, soft tissue margin was present in 61 (87%) of the 70 cases. It was also noted that it is difficult to "visualize" particular growth patterns and other features of the deep advancing tumor front, both pre- and intraoperatively, as those particularities are only evident after microscopy (5).

Positive tumor margins are strongly associated with tumor recurrence and poor patient survival. To achieve complete resection, surgeons attempt, on average, 3–4 rounds of intraoperative pathological consultations, which significantly lengthen the operative procedure. The pathological consultations require surgeons to send resected tumor margins to a histology laboratory to be processed via frozen sections. A few selected hematoxylin and eosin (H&E)-stained slides have to be evaluated quickly by a pathologist for the presence of malignant tumor cells, which requires an extra 20–30 minutes per round. Three additional potential problems that are associated with the procedure include sampling error (where the tissue is collected), false negative reading of frozen sections, and significant delay of the surgery (average of 3 rounds per head and neck cancer surgery). Intraoperative tumor imaging has the potential of allowing surgeons to clearly delineate tumor margins and assess residual disease. Transoral surgical laser resections of head and neck cancers are associated with improved postoperative function (6). If tumor margins could be accurately intraoperatively assessed, unnecessary removal of healthy tissue would be minimized, complete removal of tumors would be ensured, and neck dissection would be limited to only those cases with tumor-positive lymph nodes. An accurate assessment of tumor margins would provide the opportunity to increase survival and improve the quality of life for patients with head and neck cancer. Therefore, an improved, real-time imaging method to intraoperatively guide malignant tumor margin detection at the point-of-care is urgently needed.

Successful application in SCCHN may allow expansion of the technique to other cancers. By definition, carcinomas begin "in situ" on the epithelial side of the basement membrane and are considered to be benign as long as the cells forming them remain on this side. Eventually, however, carcinomas acquire the ability to breach the basement membrane, and individual cancer cells or groups of cancer cells begin to invade the nearby stroma (7). At the leading invasive edge, the melanoma cells display beta integrins that enable the cancer cells to attach to the extracellular matrix in front of them (8). The cyclic peptide, cyclopentapeptide cyclo(lys-Arg-Gly-Asp-phe) [c(KRGDf)], is known to target $\alpha v\beta 3$ integrin. Integrins are a family of heterodimeric glycoproteins consisting of $\alpha$ and $\beta$ subunits that noncovalently interact with form cell surface adhesion receptors. This receptor class is involved in invasive tumor cells and tumor-associated neovasculature. The cell adhesion molecule integrin $\alpha v\beta 3$ is highly expressed on tumor neovasculature and invasive tumor cells, but not on quiescent vessels or normal cells (9, 10). Thus, integrin $\alpha v\beta 3$ may be a specific biomarker of tumor neovasculature and infiltrating malignant tumor cells. In recent years, several research groups have developed a series of Arg-Gly-Asp (RGD) peptide-based positron emission tomography (PET) radiotracers for noninvasive imaging of integrin $\alpha v\beta 3$ expression to detect tumor neovasculature (11-13). Among these, F18-labeled RGD peptides are under clinical investigation in patients with cancer (14). However, RGD peptides have never been used for the detection of infiltrating tumor cells in intraoperative settings. IRDye800CW (LI-COR Biosciences, Lincoln, Nebraska) has an emission spectrum centered around 800 nm. In 2007, this dye passed animal toxicity studies using a protocol reviewed by the Food and Drug Administration (FDA). RGD peptides have already been used as PET imaging radiotracer in humans. Therefore, RGD-conjugated IRDye800CW could be readily translated to the clinical setting.

## METHODOLOGY

### Cell Culture

We established metastatic SCCHN tumor cell E3 from a poorly metastatic 686LN parental cell line by 4 rounds of in vivo selection using an orthotopic SCCHN xenograft mouse model (15).

The metastatic SCCHN cell E3 was cultured in 5% $CO_2$ at 37°C in Dulbecco's Modified Eagle's Medium/F-12 (Invitrogen, Carlsbad, California) supplemented with 10% fetal bovine serum (Sigma-Aldrich, St. Louis, Missouri), 200 mM L-glutamine, 50 U/mL penicillin, and 50 $\mu$g/mL streptomycin (Invitrogen).

### Orthotopic SCCHN Xenograft Mouse Model

Orthotopic animal experiments were performed on 6-week-old nude female mice (Harlan, Indianapolis, Indiana). We established highly metastatic SCCHN tumor cell E3 from a poorly metastatic 686LN parental cell line by 4 rounds of in vivo selection using an orthotopic SCCHN xenograft mouse model (15). The orthotopic metastatic SCCHN mouse model was described in our previous publication. In brief, we injected metastatic E3 cells ($1 \times 10^6$ cells in 50 $\mu$L phosphate buffered saline [PBS] with 10% matrigel) into the submandibular subcutaneous tissue to the mylohyoid muscle of the nude mice to create an orthotopic SCCHN xenograft. These metastatic cells not only formed large primary tumors but also spread to lymph nodes and lungs within 30 days.

### Near-Infrared Tracer

IRDye 800CW (untargeted dye, control) optical probe and IRDye 800CW RGD optical probe (LI-COR Biosciences) were used for detecting tumor margins of the infiltrating (invasive) tumors. These dyes were diluted to the concentration of 5 $\mu$M with PBS, and 100 $\mu$L was injected into each nude mouse.

### Near-Infrared Fluorescence

Before the imaging experiment, the mice bearing orthotopic head and neck tumors were intravenously injected with 0.5 nmol (per 25 g of mouse) of RGD-IRDye800CW or control-IRDye800 CW (without RGD). Further, 22 hours later, these mice were transported to the imaging suite. This room was equipped with a spectroscopic device (called SpectroPen) and illuminated by a light-emitting diode light (16, 17). The mouse was sacrificed by cervical dislocation, and we opened the skin of the anterior neck region to expose the primary tumor for visualization. Near-infrared (NIR) signals from primary tumor, lung, lymph node, and mylohyoid muscle tissue without primary tumor were detected by the spectroscopic device. The spectral data were recorded on a color video and displayed on a monitor. Collected

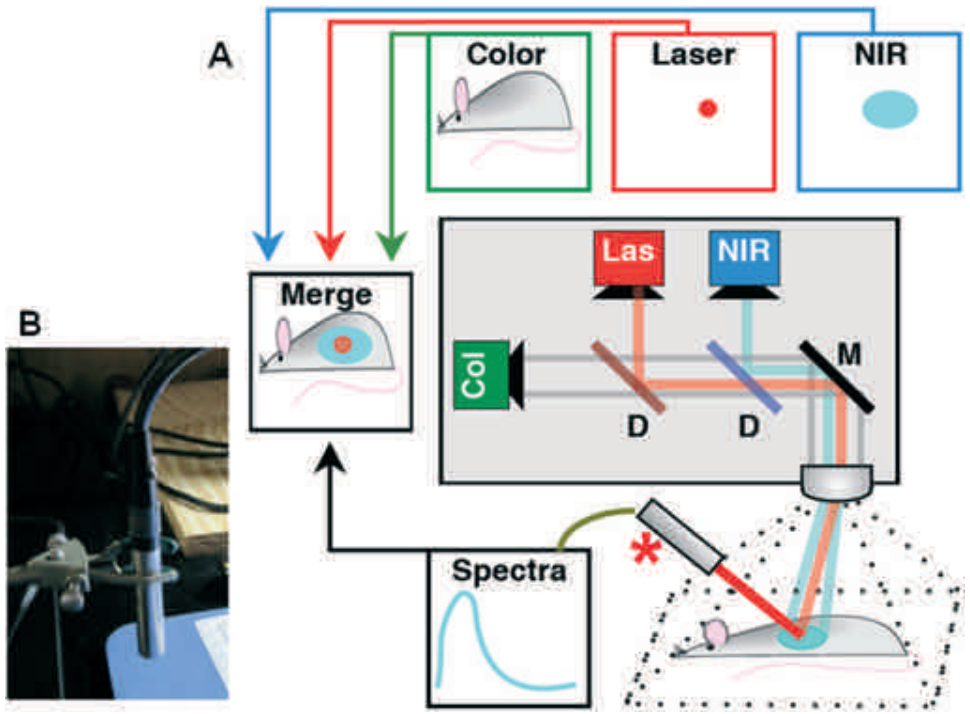


**Figure 1.** Schematic diagram adapted from Figure 1 in the study by Mohs AM et al. (Reference 16) showing the integrated spectroscopy and imaging system for near-infrared (NIR) intraoperative surgical guidance for tumor resection (A). The spectroscopic channel (provided by the SpectroPen) allows ultrasensitive detection of tumor cells at specific locations. The wide-field imaging system has 3 components, NIR channels for the probe detection (labeled NIR), a laser focal area (labeled Las), and a color video channel (labeled Col) for spatial reference. A photograph of the "pen" that is a 1- × 10-cm probe connected to a spectrometer via a 5-m fiber-optic cable (red star in Figure 1A) (B).

organ specimens were fixed in formalin and were paraffin-embedded. The paraffin-embedded specimens were sectioned into 6-$\mu$m sections and placed on glass slides and stained using H&E. All protocols for animal studies were reviewed and approved by the Institutional Animal Care and Use Committee at Emory University.

### Handheld Spectroscopic Device (SpectroPen) for Intraoperative Use

To translate RGD-IRDye800CW as an intraoperative imaging agent, we developed a pen-sized, fiber-optic probe device for spectroscopic measurements at NIR wavelengths (16). The pen is a compact 1- × 10-cm probe connected to a 5-m fiber-optic cable for both laser excitation and efficient light collection. The excitation source is a 785-nm diode laser with a focal spot of 1–2 mm on the tissue sample. It covers the spectral range of 800–930 nm with a resolution of 0.6 nm. An attached spectrometer and laptop computer instantly acquire and analyze the spectral data at a speed of 1–2 seconds. For the surgeon to monitor the entire surgical field, we have integrated the SpectroPen device with an integrated, wide-field, color/NIR imaging system (Figure 1). There are 3 optical channels that are separated by using dichroic beam splitters, which are as follows:

(1) An NIR channel for the probe.
(2) A second NIR channel for detecting the laser focal area.
(3) A color monitor channel for spatial reference.

The signals in these 3 channels are processed by a computer and are co-displayed and recorded on a color video. During a surgical procedure, the SpectroPen channel provides spectroscopic information about tumor presence or absence.

## RESULTS

### Detection of NIR Signals from a Mouse Bearing Head and Neck Tumors that Infiltrated to the Mylohyoid (Neck) Muscle and Metastasized to the Lungs

The NIR signals (color coded blue) from the bulk of the primary tumor were very strong and oversaturated the detector (Figure 2A). The NIR signal from the ear was measured to show the background from skin. This NIR signal was minimal and appeared dim blue (Figure 2B) with the same image intensity display scale. We resected the entire primary tumor, but there were residual tumors that infiltrated the mylohyoid neck muscle beyond the tumor boundaries. These residual infiltrating tumors were clearly detected by the SpectroPen device (Figure 2C). We removed the lungs from the same mouse and scanned them using the SpectroPen. Then, the NIR signals were found from the spot indicating lung metastasis (Figure 2D). Specimen of the mouse neck region without the neck bone was collected from the mouse as shown in Figure 2C and was paraffin-embedded. The paraffin block was sectioned by 6 $\mu$m and stained using H&E. The H&E-stained specimens were found to contain infil-

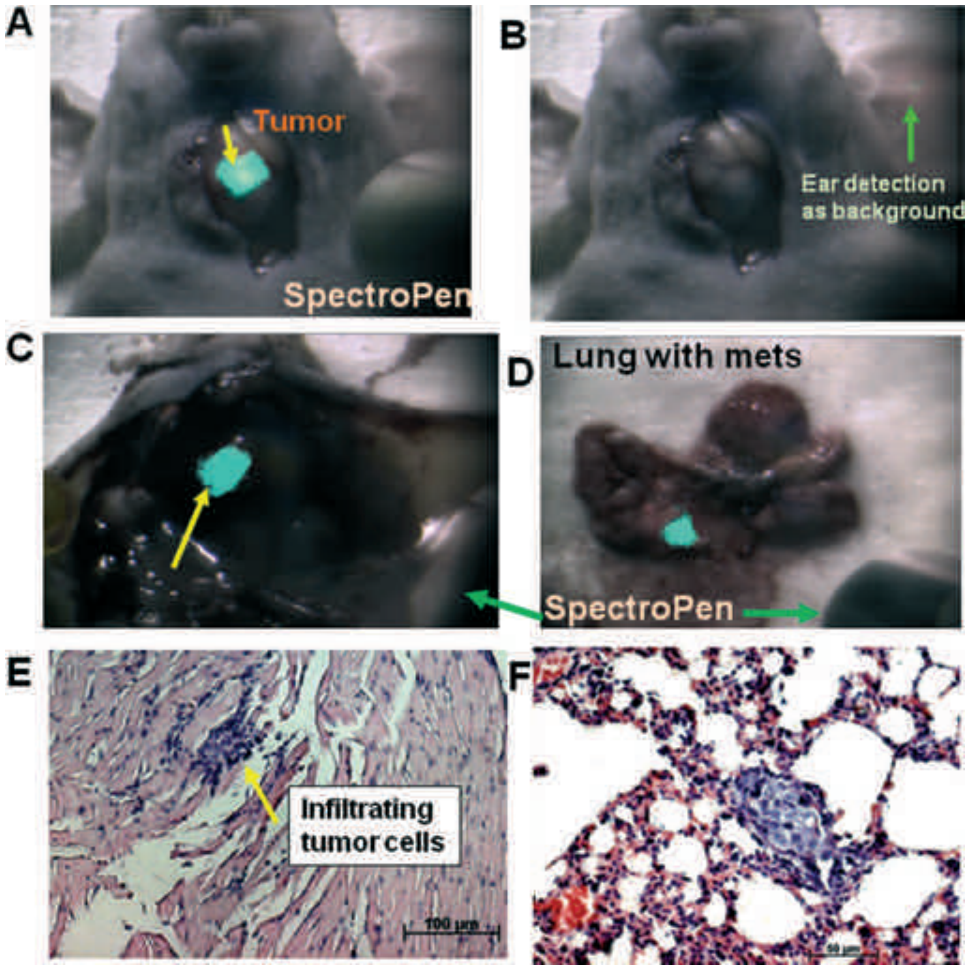


**Figure 2.** Video still of color/NIR merged images of a mouse bearing head and neck tumors that infiltrated to the mylohyoid (neck) muscle and metastasized to the lungs. The images were taken before tumor resection (A). The blue color represents intense NIR signal where the SpectroPen is pointing. The NIR signal from the ear was used as background (B). The images were taken after primary tumor resection (C). Primary tumor was resected; however, the tumors infiltrated the mylohyoid muscle. Thus, there remained residual infiltrating tumors that were easily detected by the SpectroPen. Lungs were resected, and the SpectroPen could detect NIR signal from the lungs, suggestive of lung metastasis (D). Specimens of their neck region, including residual cohorts of tumor cells (most of the bulk tumors were removed) without the neck bone, were collected and paraffin-embedded, which were sectioned by 6 $\mu$m and stained using H&E to identify infiltrating cohorts of tumor cells (where yellow arrows are pointing) (E–F).

trating tumor cells (Figure 2E). We collected specimens of the NIR-positive lung lesions and paraffin-embedded these in a certain orientation, so that we could easily identify the location of micrometastases with positive NIR signals (Figure 2F). We admit that the image–histology correlation was not performed in a fully user-unbiased manner. We also collected specimens of the NIR-positive lungs lesions and fixed these in formalin and then paraffin-embedded. The whole lungs were sectioned into 6-$\mu$m sections and placed on glass slides. Every fifth slice was scanned with the SpectroPen for NIR signals. We found that several sections were positive of the NIR signal at 805 nm (Supplemental Figure 1). NIR signal was also observed at 880 nm from the glass slide. Then, we H&E-stained the NIR-positive slides and analyzed for the presence of metastases. All the lung sections that were positive for NIR signal contained metastatic cell clusters (Supplemental Figure 1). In these samples, the average size of the metastatic cluster of tumor cells was 50–100 cells. These results indicate that it might be feasible to detect small clusters of 50–100 tumor cells in intraoperative settings.

### Detection of NIR Signals from Lymph Nodes Containing Metastatic Tumor Cells

We completely removed primary tumors from 3 mice bearing head and neck tumors, and searched NIR-positive lymph nodes by using the SpectroPen device (Supplemental Figure 2). Once the NIR signal was detected, we resected the suspicious lymph nodes, which were reconfirmed for NIR signal ex vivo. Then, positive lymph nodes were formalin-fixed and paraffin-embed-

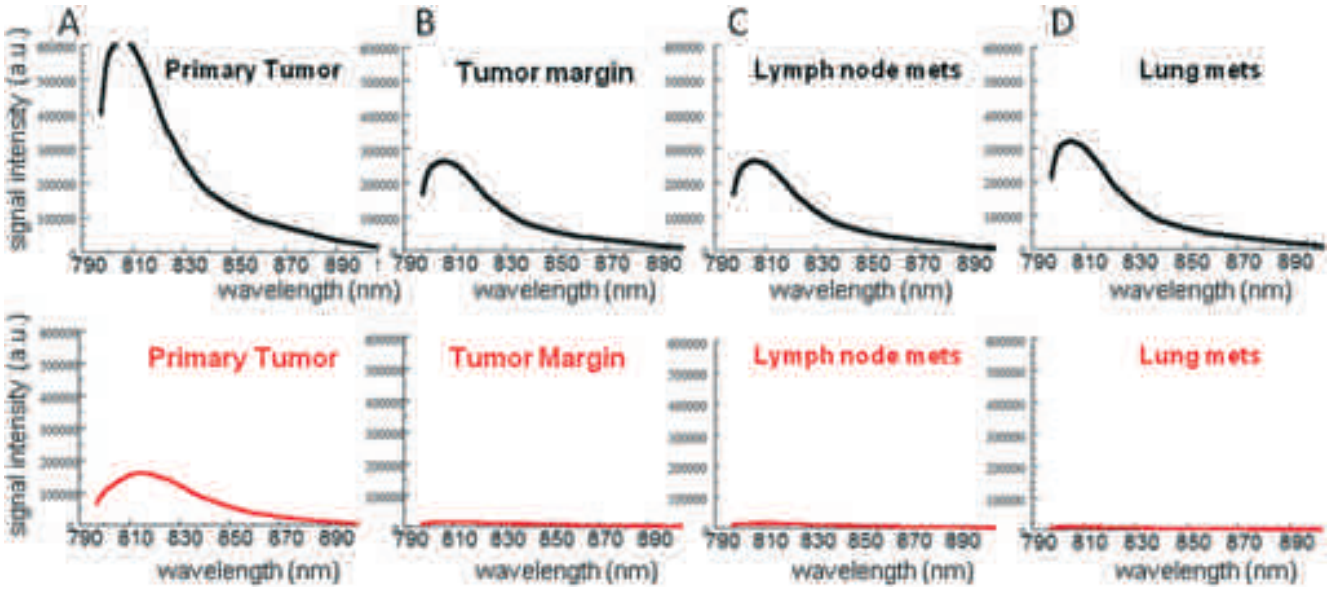


**Figure 3.** The plots of NIR spectra collected by the SpectroPen. The black spectra in the top row were collected from the mouse shown in Figure 2 (injected with RGD-IRDye800CW), whereas the red spectra in the bottom row were collected from the mouse shown in Supplemental Figure 1 (injected with IRDye800CW). NIR spectrum plots were collected from the primary tumors (A). NIR spectrum plots were collected from the mylohyoid muscle following removal of primary tumors (beyond the primary tumor margin/border), representing the presence of residual infiltrating tumors beyond the tumor boundary (B). The plots were obtained from the involved lymph node with tumor cells (C). The plots were collected from the lungs with metastases (D).

ded for histological validation, and we found that 8 out of 8 lymph nodes contained infiltrating tumor cells.

### Spectra from the SpectroPen

Figure 2 shows the representative NIR spectra of the primary tumor, infiltrating clusters of tumor cells in mylohyoid tissues at tumor margin, tumor-involved lymph node, and lung with micrometastases. The upper spectra in black traces were obtained from RGD-IRDye800CW-injected mice, whereas the bottom spectra in red traces were obtained from control IRDy800CW-injected mice. RGD-IRDye800CW-injected mice exhibited strong, saturating NIR signals from the bulk primary tumors, whereas IRDye800CW-injected mice exhibited weak NIR signals from the bulk primary tumors (Figure 3A). Once the bulk primary tumors were removed, we could easily detect the NIR signals from the invasive clusters of tumor cells in the mylohyoid muscle tissues of RGD-IRDye-injected mice (Figure 3B). But when the IRDye800CW was used, we were unable to detect the NIR signals. We also detected NIR signals from the lymph nodes and lungs of the RGD-IRDye800CW-injected mouse (Figure 3, C and D, upper panel), but could not detect the NIR signal from lymph nodes and lungs of IRDye800CW-injected mice (Figure 3, C and D, bottom panel).

### Detection of NIR Signals from a Nonmetastatic (Encapsulated) Tumor

A mouse bearing a medium-sized tumor was intravenously injected with 0.5 nmol of RGD-IRDye800CW, and 22 hours later, this mouse was sacrificed by $CO_2$ asphyxiation followed by cervical dislocation; the skin on the anterior neck region was opened to expose the tumor for visualization. The tumor was encapsulated within a boundary (Figure 4A), and had not yet infiltrated beyond the boundary of the tumor into the neck muscle. Once the tumor was completely removed, we could not detect any NIR signals from the neck area and the lung as shown in Figure 4, B and C. The collected lung specimens were formalin-fixed and paraffin-embedded. In addition, we could not find tumor cells in H&E-stained lung specimens (data not shown). From another mouse bearing a similar-size tumor, we partially removed the tumor and collected specimens from the neck region without the neck bone for histological evaluation. From H&E-stained specimens, we could not find infiltrating clusters of tumor cells beyond the tumor boundary into the neck muscle (Figure 4D), consistent with the lack of NIR signals in Figure 4B.

### Detection of NIR Signals from Control IRDye

For the control experiment, we injected the control IRDye800CW (without RGD conjugation) in a mouse bearing a large tumor. The primary tumor had a weak NIR signal (Supplemental Figure 3A). After removal of the primary tumors, there were residual infiltrating tumors; however, we could not detect NIR signals from these cells (Supplemental Figure 3B). In addition, we could not detect any NIR signal from the lungs (Supplemental Figure 3C) despite the presence of H&E-stained specimen-confirmed lung metastases (Supplemental Figure 3D).

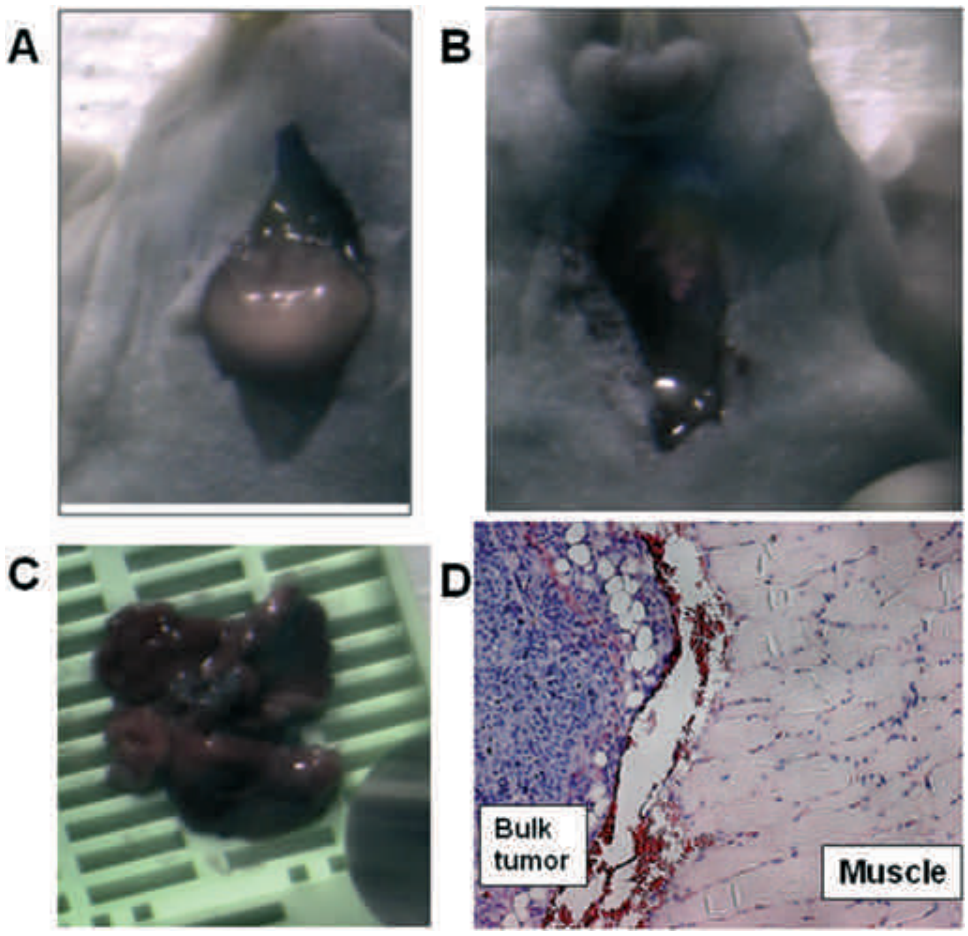


**Figure 4.** Video still of color/NIR merged images of a mouse bearing head and neck tumors that is well circumscribed as a negative control. When the tumor size is not large enough, tumor cells are encapsulated (confined), and there were no infiltrating tumor cells unlike the mouse shown in Figure 2 (A). With the tumor removal, there remained no residual tumors and no NIR signal was detected (B). For this stage of tumor development, lung metastasis is yet to occur (C). As anticipated, its lungs did not have any NIR signal detectable by the SpectroPen. H&E staining of the neck region from the same mouse: tumor cells have not infiltrated the mylohyoid neck muscle beyond the tumor boundary (D). Specimens from their neck region, including partial tumors (most of the bulk tumors were removed) without the neck bone, were collected, formalin-fixed, and paraffin-embedded, which were then sectioned by 6 $\mu$m for H&E staining. No infiltrating cohort of tumor cells was found.

## DISCUSSION

In contrast to radionuclides used in radioimmunoscintigraphy, fluorophores have no finite half-life and can be excited with light to produce multiple emissions. This is advantageous for the following 2 reasons:

(1) The optical imaging probe can be synthesized and stored nearly indefinitely, unlike radionuclides with finite half-lives.
(2) Imaging of infiltrating clusters of tumor cells can be carried out in 24–48 hours following systemic administration of the optical imaging probes because infiltrating clusters of 50–100 cells have not developed (or associated with) leaky neovasculature.

Therefore, the optical probe may require 24–48 hours to reach the target cells in human. Thus, radionuclides with a half-life of 2–6 hours will be inappropriate for the purpose. The NIR wavelength range between 650 and 950 nm is considered a "clear window" for in vivo imaging because of reduced blood absorption, tissue scattering, and autofluorescence (18). IRDye800CW (LI-COR Biosciences) with fluorescence emission centered around 800 nm is a commercially available NIR dye with functional groups for conjugation, and it has passed animal toxicity studies using a protocol reviewed by the FDA in 2007 (https://www.licor.com/clinical_translation/index.html).

Houston et al. have compared optical imaging with nuclear imaging by using cyclic RGD conjugated with a dual-labeled probe with a radiotracer ($^{111}$indium) for gamma scintigraphy and with RDye800CW (19). Image acquisition time was 15 minutes for the gamma scintigraphy images and 800 milliseconds for the optical images acquired using an intensified charge-coupled device-equipped whole-body animal imager. Their results show that the signal-to-noise ratio (SNR) was significantly higher for optical than nuclear imaging. Furthermore, an anal-

ysis of signal-to-noise versus contrast showed greater sensitivity of optical over nuclear imaging for subcutaneous tumor targets. Their work strongly supports that IRDye800CW offers a potentially better tracer than radioisotopes for intraoperative guidance. Furthermore, Sampath et al. used a similar dual-label approach using trastuzumab (Herceptin®, Genentech, Inc.) (20) in subcutaneous xenograft models to show enhanced SNRs in NIR fluorescence compared with nuclear imaging. Because subcutaneous xenograft models offer shallow penetration depths, the results may be as expected and similar to what might be encountered for intraoperative guidance where the surgical fields are exposed.

Characterization of RGD-IRDye800CW, including in vitro and in vivo binding to a variety of tumor cell lines (ie, U87, A431, PC3M-LN4, and 22Rv1), was reported by Kovar et al. in collaboration with LI-COR Bioscience at the American Association for Cancer Research Annual Meeting (http://biosupport.licor.com/docs/IntegrinSpecNIRImagingv2_AACR09_JK.pdf). Specificity of the conjugate for the integrin receptor was confirmed by competition with either an unlabeled RGD peptide or unlabeled RAD (Arg-Ala-Asp), nonspecific peptide in U87 cells. In addition, whole-body animal images confirmed that RGD-IRDye800CW maintains specificity to the target tissue when tested for in vivo applications. Images of nude mice bearing 2 subcutaneously implanted tumors on the rear flank show that RGD-IRDye800CW localized to tumor tissues. A dose of unlabeled RGD (given intravenously via the tail vein) before RGD-IRDye800CW resulted in reduced signals in both tumors, confirming specificity.

We established metastatic SCCHN cells that not only form large primary tumors but also spread to lymph nodes and lungs within 30 days. RGD conjugated with IRDyeCW800 or IRDyeCW800 without RGD conjugation was intravenously injected 22 hours before the imaging experiment. From our preliminary studies, we found that 22 hours following the injection of 0.5 nmol of RGD-IRDye800CW provided us with the best tumor-to-muscle uptake ratio of RGD-IRDye800CW. In addition, data from LI-COR Biosciences (http://biosupport.licor.com/docs/IntegrinSpecNIRImagingv2_AACR09_JK.pdf) also support a 22-hour waiting period before imaging, as the best SNR with a reasonably good background clearance was obtained at 22 hours post injection of RGD-IRDye800CW. It is worth noting that another important biomarker for head and neck tumors is the epidermal growth factor receptor (EGFR). Head and neck cancer has the highest rate of EGFR overexpression compared with other cancers (21, 22). Cetuximab, a monoclonal antibody directed against the EGFR, is effective in treating head and neck cancer when used alone or in combination with radiotherapy and has recently been approved by the FDA for head and neck cancer (23). An EGFR-targeted NIR dye may also have excellent potential as an intraoperative imaging probe, which can be evaluated in future studies to expand the available number of dyes (24). This would further improve the possible clinical applications along with additional molecular diagnostic specificity for using this point-of-care technology in the surgical suite.

To conclude, we have reported the combination of a targeted NIR tracer, a handheld spectroscopic pen device, and a multichannel wide-field imaging system for highly sensitive detection of the integrin $\alpha v\beta 3$, which is overexpressed by tumor neovasculature and invading tumor cells, but not by quiescent vessels or normal cells. By using a metastatic orthotopic head and neck cancer animal model, we have shown that this combination allows intraoperative detection of both invasive tumor margins and metastatic lymph nodes and lungs. Correlated histological data further indicate that microscopic clusters of 50–100 tumor cells can be detected intraoperatively, raising new possibilities in guiding surgical resection of microscopic tumors and metastatic lymph nodes. In comparison with other imaging modalities such as computed tomography, PET, or magnetic resonance imaging, this optical imaging technology is highly sensitive and molecularly specific, but its tissue penetration depth is currently limited to about 3–5 mm, so deeply buried or hidden tumor nodules cannot be detected under in vivo or intraoperative conditions. This problem can be overcome or alleviated by recent advances in photoacoustic imaging and NIR fluorescence in the second NIR window (between 1000 and 1700 nm in wavelength), which have shown that the tissue penetration depth could be considerably (by 5- to 10-fold) improved in comparison with optical imaging in the first NIR window (650–950 nm) (25-27).

## Supplemental Materials

Supplemental Figures 1-3: http://dx.doi.org/10.18383/j.tom.2016.00253.sup.01

## ACKNOWLEDGMENTS

This work was supported by grants from the National Cancer Institute (R01CA165306 to H.S., R01CA163256 to S.N., and K99CA153916 to A.M.). The authors thank Ms. Amber Feng for assistance in proofreading the manuscript.

Disclosure: Mohs AM, Mancini MC, and Nie S are inventors of instrumentation related to this manuscript.

Conflict of Interest: None reported.

## REFERENCES

1. Sanderson RJ, Ironside JA. Squamous cell carcinomas of the head and neck. BMJ. 2002;325(7368):822–827.
2. Kotwall C, Sako K, Razack MS, Rao U, Bakamjian V, Shedd DP. Metastatic patterns in squamous cell cancer of the head and neck. Am J Surg. 1987;154(4):439–442.
3. Casiglia J, Woo SB. A comprehensive review of oral cancer. Gen Dent. 2001;49(1):72–82.
4. Ravasz LA, Slootweg PJ, Hordijk GJ, Smit F, van der Tweel I. The status of the resection margin as a prognostic factor in the treatment of head and neck carcinoma. J Craniomaxillofac Surg. 1991;19(7):314–318.
5. Woolgar JA, Triantafyllou A. A histopathological appraisal of surgical margins in oral and oropharyngeal cancer resection specimens. Oral Oncol. 2005;41(10):1034–1043.
6. Puxeddu R, Piazza C, Mensi MC, Ledda GP, Argiolas F, Peretti G. Carbon dioxide laser salvage surgery after radiotherapy failure in T1 and T2 glottic carcinoma. Otolaryngol Head Neck Surg. 2004;130(1):84–88.
7. Friedl P, Hegerfeldt Y, Tusch M. Collective cell migration in morphogenesis and cancer. Int J Dev Biol. 2004;48(5-6):441–449.
8. Weinberg, RA. The Biology of Cancer. 1st ed. New York, NY: Garland Science; 2007:592.

9. Eliceiri BP, Cheresh DA. The role of αv integrins during angiogenesis: insights into potential mechanisms of action and clinical development. J Clin Invest. 1999; 103(9):1227–1230.
10. Friedlander M, Theesfeld CL, Sugita M, Fruttiger M, Thomas MA, Chang S, Cheresh DA. Involvement of integrins alpha v beta 3 and alpha v beta 5 in ocular neovascular diseases. Proc Natl Acad Sci USA. 1996;93(18):9764–9769.
11. Haubner R, Kuhnast B, Mang C, Weber WA, Kessler H, Wester HJ, Schwaiger M. [18F]Galacto-RGD: synthesis, radiolabeling, metabolic stability, and radiation dose estimates. Bioconjug Chem. 2004;15(1):61–69.
12. Zhang X, Xiong Z, Wu Y, Cai W, Tseng JR, Gambhir SS, Chen X. Quantitative PET imaging of tumor integrin alphavbeta3 expression with 18F-FRGD2. J Nucl Med. 2006;47(1):113–121.
13. Jeong JM, Hong MK, Chang YS, Lee YS, Kim YJ, Cheon GJ, Lee DS, Chung JK, Lee MC. Preparation of a promising angiogenesis PET imaging agent: 68Ga-labeled c(RGDyK)-isothiocyanatobenzyl-1,4,7-triazacyclononane-1,4,7-triacetic acid and feasibility studies in mice. J Nucl Med. 2008;49(5):830–836.
14. Haubner R, Weber WA, Beer AJ, Vabuliene E, Reim D, Sarbia M, Becker KF, Goebel M, Hein R, Wester HJ, Kessler H, Schwaiger M. Noninvasive visualization of the activated alphavbeta3 integrin in cancer patients by positron emission tomography and [18F]Galacto-RGD. PLoS Med. 2005;2(3):e70.
15. Yoon Y, Liang Z, Zhang X, Choe M, Cho HT, Shin DM, Goodman M, Chen Z, Shim H. CXCR4 antagonist blocks both growth of primary tumor and metastasis of head and neck cancer in xenograft mouse models. Cancer Res. 2007;67(15): 7518–7524.
16. Mohs AM, Mancini MC, Provenzale JM, Saba CF, Cornell KK, Howerth EW, Nie S. An integrated widefield imaging and spectroscopy system for contrast-enhanced, image-guided resection of tumors. IEEE Trans Biomed Eng. 2015;62(5):1416–1424.
17. Mohs AM, Mancini MC, Singhal S, Provenzale JM, Leyland-Jones B, Wang MD, Nie S. Hand-held spectroscopic device for in vivo and intraoperative tumor detection: contrast enhancement, detection sensitivity, and tissue penetration. Anal Chem. 2010;82(21):9058–9065.
18. Weissleder R, Tung CH, Mahmood U, Bogdanov A, Jr. In vivo imaging of tumors with protease-activated near-infrared fluorescent probes. Nat Biotechnol. 1999; 17(4):375–378.
19. Houston JP, Ke S, Wang W, Li C, Sevick-Muraca EM. Quality analysis of in vivo near-infrared fluorescence and conventional gamma images acquired using a dual-labeled tumor-targeting probe. J Biomed Opt. 2005;10(5):054010.
20. Sampath L, Kwon S, Ke S, Wang W, Schiff R, Mawad ME, Sevick-Muraca EM. Dual-labeled trastuzumab-based imaging agent for the detection of human epidermal growth factor receptor 2 overexpression in breast cancer. J Nucl Med. 2007;48(9):1501–1510.
21. Pomerantz RG, Grandis JR. The epidermal growth factor receptor signaling network in head and neck carcinogenesis and implications for targeted therapy. Semin Oncol. 2004;31(6):734–743.
22. Rogers SJ, Harrington KJ, Rhys-Evans P, P OC, Eccles SA. Biological significance of c-erbB family oncogenes in head and neck cancer. Cancer Metastasis Rev. 2005;24(1):47–69.
23. Bonner JA, Harari PM, Giralt J, Azarnia N, Shin DM, Cohen RB, Jones CU, Sur R, Raben D, Jassem J, Ove R, Kies MS, Baselga J, Youssoufian H, Amellal N, Rowinsky EK, Ang KK. Radiotherapy plus cetuximab for squamous-cell carcinoma of the head and neck. N Engl J Med. 2006;354(6):567–578.
24. Gleysteen JP, Newman JR, Chhieng D, Frost A, Zinn KR, Rosenthal EL. Fluorescent labeled anti-EGFR antibody for identification of regional and distant metastasis in a preclinical xenograft model. Head Neck. 2008;30(6):782–789.
25. Smith AM, Mancini MC, Nie S. Bioimaging: second window for in vivo imaging. Nat Nanotechnol. 2009;4(11):710–711.
26. Weissleder R. A clearer vision for in vivo imaging. Nat Biotechnol. 2001;19(4): 316–317.
27. Zhang HF, Maslov K, Stoica G, Wang LV. Functional photoacoustic microscopy for high-resolution and noninvasive in vivo imaging. Nat Biotechnol. 2006;24(7): 848–851.